Development of a Mold Cracking Simulator: The Study of Breakout and Crack Formation in Continuous Casting Mold

YEXIN ZHANG, WANLIN WANG, and HAIHUI ZHANG

Based on the mold simulator technology, a mold-cracking simulator has been successfully developed to study the process of breakout and the shell surface crack formation during the initial solidification of molten steel inside the continuous casting mold. First, a spheroidal protrusion was installed on the mold hot surface to mimic the abnormal force that generated by mold wall deformation, and then the external force was applied to the initial solidified shell, to facilitate the formation of breakout and shell surface cracks. Second, the responding temperature and heat flux across mold hot surface were recovered by an inverse heat conduction problem. The experimental results indicated that the mold breakout occurs around the shell tip by the combined efforts from external horizontal force, ferrostatic pressure, and thermal stresses during positive strip time. The breakout tends to introduce the peak of the responding temperature and heat flux across the mold hot surface. The vertical propagation velocity of the rupture point in the solidification shell has been calculated as 0.42 m/s in this study, which is in good agreement with industrial slabs. The paper also suggested that surface transverse crack formation is related to the segregation of sulfur during the initial solidification of molten steel.

I. INTRODUCTION

Obviously, a breakout in the process of continuous casting would not only cause the loss of production, but also introduce the severe safety issues. Breakouts are broadly classified into two categories: hanging- or sticking-type breakout[1–3] caused by improper lubrication between mold and strand, and cracking-type breakout caused by longitudinal corner crack and broad face longitudinal cracks in the strand. Intensive research has been conducted for the detection and prevention of breakouts. The method based on mold/strand friction has been proved to be a successful way for the detection of sticking-type breakout, while the detected signals sometimes might be false because the friction is associated with complicated mold flux infiltration in the copper mold during continuous casting. Other breakout prediction systems are based on the recording temperature signals[4] or coupled with mathematical calculation.[5] However, these methods can only detect the risk of breakout, and the variation of heat transfer, responding temperatures, as well as the association with the mold movement is still not clear.

Meanwhile, mold flux entrapment, solute segregation, oscillation marks, *etc.*[6,7] have great influence on the surface quality of the cast products, and the corresponding surface cracks tend to affect the hot ductility of steels and introduce potential breakouts occurred in the casting process.[8,9] Brimacombe[10] reviewed that the formation of most surface cracks is within a high-temperature zone: 1613 K (1340 °C) to the solidus temperature, as the strength and ductility are relatively low in this region, due to the presence of liquid films in the interdendritic regions[11]; they further indicated that transverse cracks may result from excessive friction in the mold.

The transverse cracks are usually found along the oscillation marks (OMs), and Weisgerber[12] has investigated the relationship between the crack formation and the different types of oscillation marks; the research suggested that the segregation of solute elements has been found at the bottom of deeper OMs and it would further cause the primary crack at the bottom of the OMs. Besides, coarser austenite grain has been confirmed to reduce the hot ductility of slab and enhance the cracking of slab surface.[13,14] In order to improve the hot ductility of the slab, Kato[15] controlled the cooling temperature during the second cooling zone with the aim to refine the slab surface microstructure.

However, most of these studies focus on the slab samples that have been processed through secondary cooling and bending segment. Very few researches have been conducted to study the origin of the crack formation during the initial solidification in the mold,

YEXIN ZHANG, Graduate Student, WANLIN WANG, Professor, Director, and HAIHUI ZHANG, Post Doctor, are with the School of Metallurgy and Environment, Central South University, Changsha 410083, China, and also with the National Center for International Research of Clean Metallurgy, Central South University, Changsha 410083, China. Contact e-mail: wanlin.wang@gmail.com

as the formation of the cracks in the copper mold is hardly observed due to the restriction of the continuous caster. Recently, Santillana[16] designed a mold cracking simulator to simulate the cracks formation process by applying external forces on the initial solidified shell; however, the forces imposed on shell were after the mold was pulled out of the liquid bath.

In this study, a mold cracking simulator has been successfully developed based on the previous mold simulator technique,[17–20] through the installation of a spheroidal protrusion on the hot surface of the copper mold. This newly developed simulator will allow the clear investigation of the interrelationship between the mold breakouts, variance of responding of heat flux and temperature, mold oscillation and surface crack formation.

II. EXPERIMENTAL APPARATUS AND PROCESS

A. Description of the Mold Cracking Simulator

The mold cracking simulator system applied in this study is an inverse-type water-cooled copper mold (30 mm × 50 mm × 350 mm) with oscillation ability and its schematic figuration is shown in Figure 1. The whole system includes 7 units: copper mold with a spheroidal protrusion on the hot surface, heating furnace, water-cooling system, shell withdrawal (extractor) system, mold oscillator system, data acquisition/control system, and stage driver unit to descend/ascend the mold system in/out of melt pool. The cooling system is a 'U'-type water-cooling pipe manufactured along the center line of copper plate, 12.5 mm away from both ends and gets connected 20 mm above the bottom. The copper mold is equipped with an extractor system that makes only one face of the mold expose to the liquid melt. As the liquid steel contacts with the hot surface of the water-cooled mold, it would solidify and form the initial shell, the extractor then withdraws the solidifying shell downward, and the fresh liquid steel would contact with mold for subsequent solidification that is similar to the dummy bar does at the start-up of a continuous casting operation. The cast speed/length can be controlled by the extractor system and the stroke/frequency is controlled by the mold oscillator system.

In order to *in situ* observe the transient variation of the temperatures and heat fluxes during the initial shell solidification, two columns of 16 K-type thermocouples are embedded along the centerline of the outlet water pipe. They are 5 mm apart vertically, and 3 mm (the first column of thermocouple, termed 'Hot') and 8 mm (the second column of thermocouple, termed "Cold") horizontally away from the hot surface of the mold (see in Figure 2) to acquire the responding temperature data during the test. The distribution of the thermocouples is based on our previous study[19,20] and is shown in Figure 2. The label TC refers to the thermocouple, S represents mold surface and the number means the location on the copper mold. For example, TC1 refers to the location of the first row of thermocouples and S1 refers to the location on the hot surface paralleled to the first row.

The data acquisition system was used to record the responding temperature during the test, and the sampling frequency is 60 Hz. With these temperature signals, the responding in-mold hot surface temperatures and the heat fluxes can be calculated through a two-dimensional inverse heat conduction problem (2D-IHCP).[21] The 2D-IHCP is capable of restructuring the mold wall temperature and heat flux across mold surface from the in-mold temperature measurement and shows a good anti-interference ability of inverse results to the temperature measurement noise.

The copper mold designed here is to generate cracks under continuous casting conditions by equipped a spheroidal protrusion on the hot surface of the water-cooling copper mold as shown in Figure 2. The radius of the spheroidal protrusion is 3 mm, which is located at the 2/3 width and 50 mm above the bottom of the copper mold. The protrusion is used to increase the friction forces between the initial solidified shell and the mold hot surface, which would introduce extra force to generate cracks or even breakout of the initial shell during continuous casting.

B. Experiment Process and Results

Typical experiments were conducted to investigate the process of breakout and the shell surface crack formation at the initial stage of solidification inside the continuous casting mold by using this mold cracking simulator technique.

During the experimental process, 25 kg medium carbon steel ([C] 0.18 pct, [Si] 0.58 pct, [Mn] 1.18 pct, [P] 0.036 pct, and [S] 0.034 pct) was melted in the induction furnace. When the temperature of the melt was adjusted to the target value (to control the superheat), about 0.5 kg mold flux (composition is listed Table I) was added on the top of liquid steel. After the flux was melted, the water-cooled copper mold covered with an extractor was lowered into the melt with a preset depth that makes the liquid level of melt located in the mold thermocouple-measuring zone, while the mold started to oscillate with a sinusoidal manner. Subsequently, the mold and extractor were held for a few seconds to form an initial shell on the mold surface to insure that the initial shell was strong enough to be dragged downward. Next, the progress of continuous casting stage started, and the extractor dragged the solidifying shell downward for 50 mm at a constant speed (equals to the continuous casting speed). During the casting process, the initial solidified shell would touch the protrusion and was subjected to the extra friction force, which would result in the formation of breakouts and surface cracks. When the continuous casting was completed, the mold oscillation was stopped and then withdrawn out of the furnace and cooled in the air. The cast parameters for the mold simulator run are listed in Table II. The detailed information about experimental procedure has been described by Zhang et al.[19]
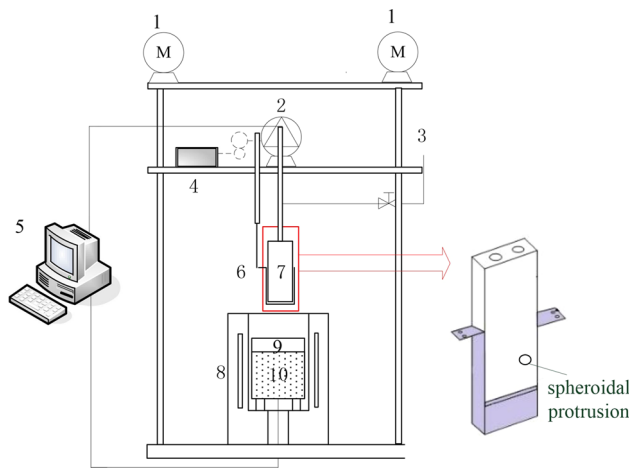
Fig. 1—Schematic figure of mold simulator 1-stages drive; 2-oscillator motor; 3-cooling water; 4-extractor motor; 5-data acquisition/control system; 6-extractor; 7-copper mold; 8-induction coil; 9-mold flux; 10-melt.[19]

The measured responding temperatures of the thermocouples are shown in Figure 3, where the locations of the thermocouples (TCs) are shown in Figure 2, and TC2 corresponds to the location of the liquid steel level. TC1 represents the location 5 mm above the liquid steel level, and TC7 corresponds to the location of spheroidal protrusion. The measured temperatures could be divided into four stages according to the process of the experiment. During stage I (before 38.9 seconds), as the mold dips into the melt bath, the lower part of the mold would contact with the liquid melt firstly and the responding temperature increases sequentially. As it enters into stage II (38.9 to 39.9 seconds) when the mold is kept in the bath for only one second to form the initial shell, the responding temperatures increase continuously. During the Stage I and II, the melt steel first contacts with the hot face, then a huge temperature gradient forms between the melt and mold, the liquid melt would quickly solidify against the mold surface, hence the responding temperatures in the mold increase
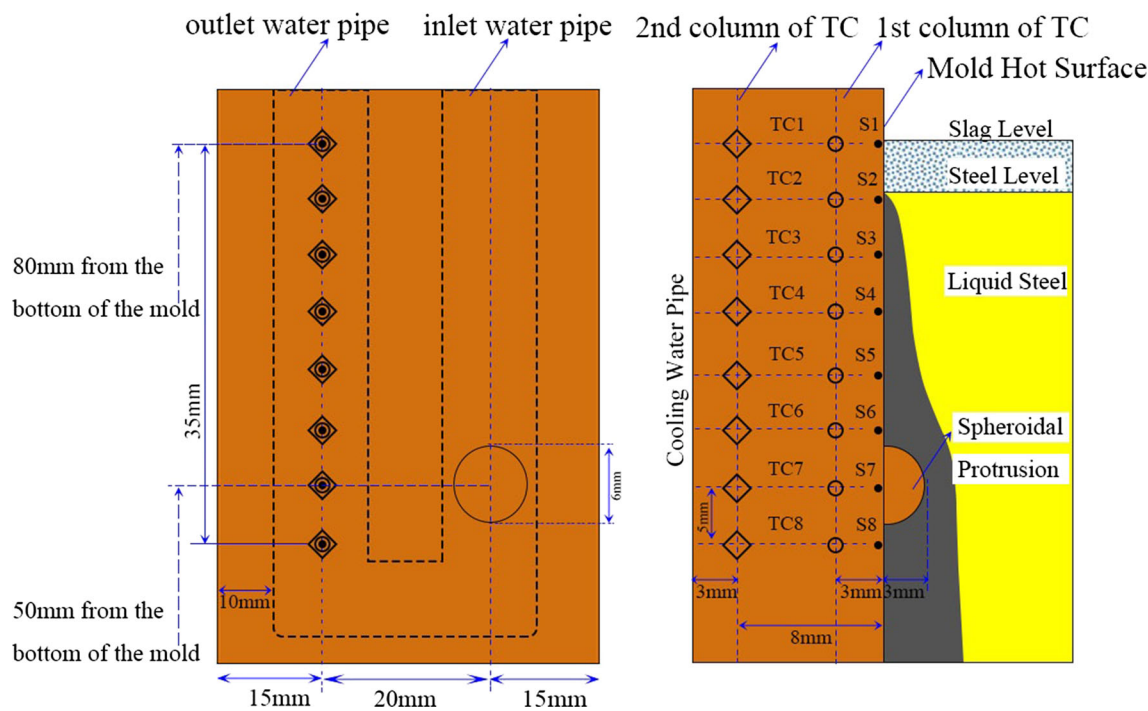

Fig. 2—Geometry of the mold and the location of thermocouples.

Table I. The Major Composition of Mold Flux, Weight Percent

CaO	SiO$_2$	MgO	Al$_2$O$_3$	Na$_2$O	Li$_2$O	F	Cao/SiO$_2$ e
43.06	34.44	2	4	7.5	1	8	1.25

Table II. The Cast Parameters During the Continuous Casting

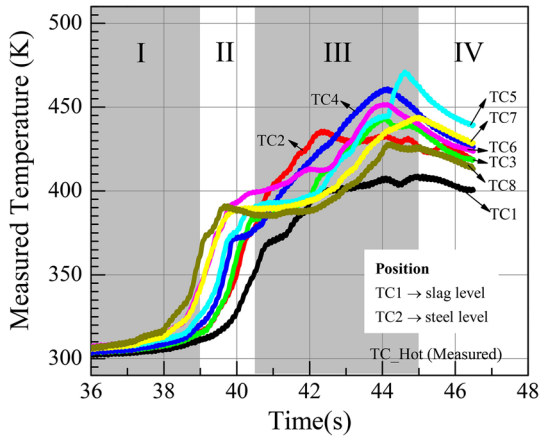| Pouring Temperature (K)	Cast Length (mm)	Cast Speed (mm/s)	Stroke (mm)	Frequency (Hz)
1818 K (1545 °C)	5	10	8	1.67

Fig. 3—The responding in-mold wall temperatures measured by 1st column thermocouple.
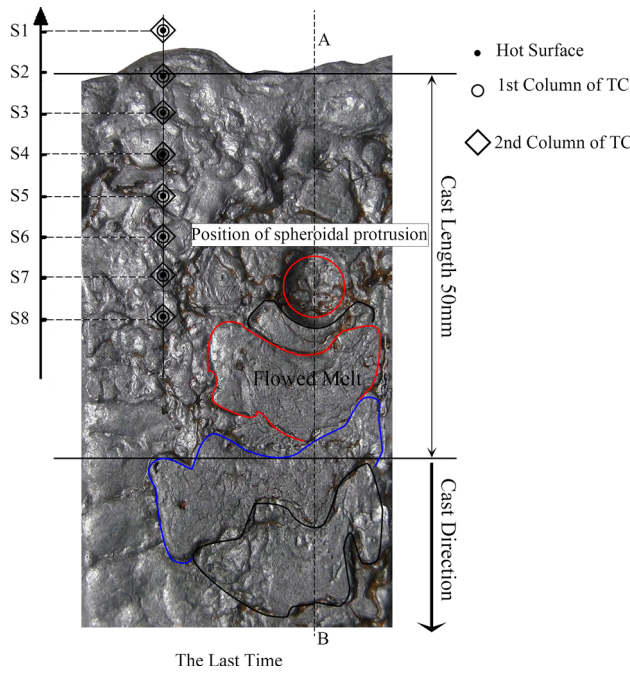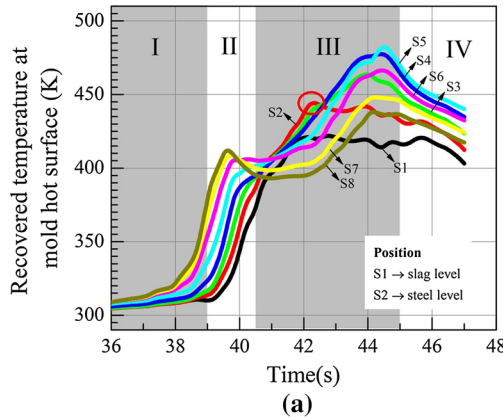

The Last Time

Fig. 4—The solidified shell surface profile from the experiment.

dramatically. During the stage III (39.9 to 45.5 seconds), the initial shell is then withdrawn downward by the extractor at a constant speed of 10 mm/s, and the responding temperatures are very complex, which will be described in details in Figure 5.

Once the cast is completed, the mold system is drawn out of the melt bath and cooled in the air; thus, the responding temperatures decrease during the stage IV. Finally, Figure 4 shows the surface profile of the shell that has been cast from the mold simulator experiment. It could be observed that the shell surface is not smooth, which might be caused by the re-solidified melt flow through the rupture of the original shell surface due to the breakout in the cast process, and this part will be discussed later. It can also be seen that the transverse cracks grow along the bottom of the oscillation marks.

III. ANALYSIS AND DISCUSSION

A. Temperatures and Heat Fluxes

Figure 5 shows the mold hot surface temperatures recovered by a 2D-IHCP mathematic model[21] from the in-mold responding temperature measurements
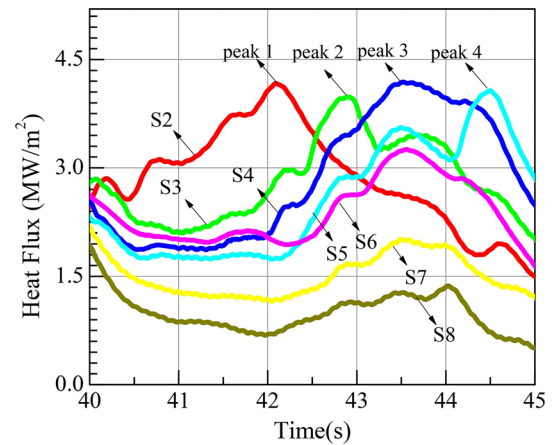

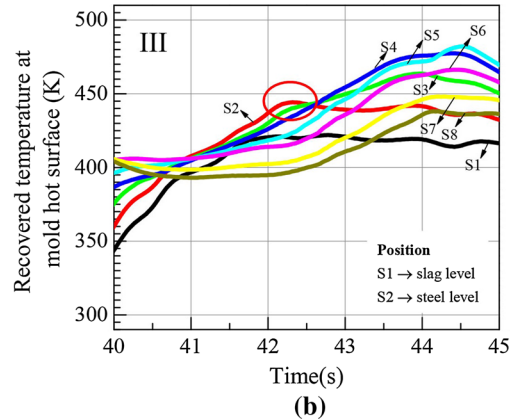Fig. 6—Evolution of mold hot surface heat fluxes during continuous casting.

Fig. 5—The recovered temperatures across the mold hot surface: (a) during the test, and (b) during casting stage III.

(Figure 3), where the S positions on hot surface are shown in Figure 2. It shows the similar trend as the responding temperature histories that measured by the 1st column thermocouples as shown in Figure 5(a).

In order to analyze the detailed hot surface temperatures behavior during the initial casting, the responding temperatures' histories in Stage III are extracted and shown in Figure 5(b). It was observed that the mold surface temperatures for the location above liquid steel level (S1, 5 mm above, slag level) first increase from 39.9 to 42 seconds and then comes to a relatively steady state that is similar to the trend of S2. This is because the process of stage II is just hold for one second, and the initial shell continuous to grow and the latent heat is

further released. After 42s, the heating potential is equal to the cooling potential, i.e., the system steps into a relative steady state. The temperature of S2 on the mold hot surface is located around the liquid steel level, and it also increases from 39.9 to 41.7 seconds firstly. However, its value is kept on increasing to the peak at 42.5 seconds (circled in Figure 5(b)), and then slightly decreases to steady state. It turns out that the initial shell rupture is occurred near/below S2 between 41.7 and 42.5 seconds, and then a little amount of fresh melt flows into the gap between the mold hot surface and the shell leading to the peak of S2. Therefore, the mold hot surface bellow S2 is heated by this infiltration, and the corresponding temperatures of S3, S4, and S5 increase after 42 seconds.

For the temperatures of S6, S7, and S8 where they are located around the spheroidal protrusion, they firstly decrease from 40 to 42 seconds, which is due to the fact that the spheroidal protrusion provides an extra force on the shell and push the shell toward the melt slightly; thus, the gap between the mold hot surface and shell is enlarged leading to the increase of interfacial thermal resistance. After that the responding temperatures increase with the infiltration of fresh melt due to the formation of breakouts.

In order to further analyze the variation of mold hot surface heat flux introduced by the breakouts, the responding heat flux across the mold hot surface during the stage of casting is then calculated by the measured responding temperature histories through 2D-IHCP and given in Figure 6. It is found that the variation of the heat fluxes shows a similar variation pattern as that of the hot surface temperatures. It is clearly shown that the heat flux of S2 near the meniscus increases first and peaks around 4 MW/m^2 at 42.2 seconds, and then decrease afterwards, which is due to the fact that the mold hot surface is continued to be heated through the melt core from 39.9 to 42 seconds. Then the shell ruptures at S2 position around 42 seconds and the fresh
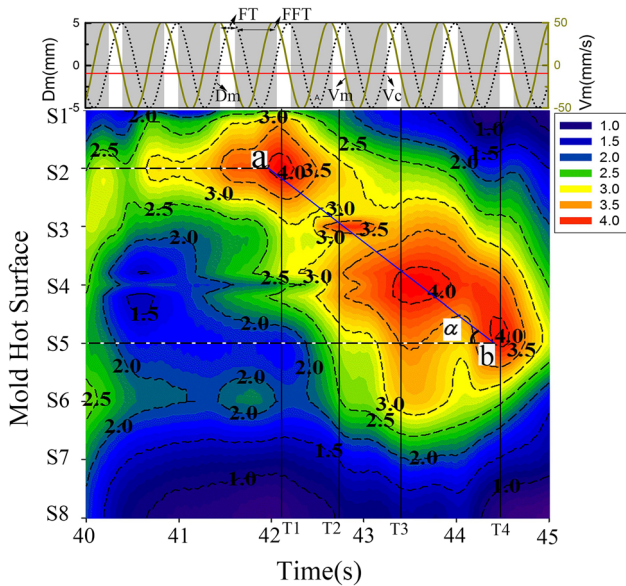

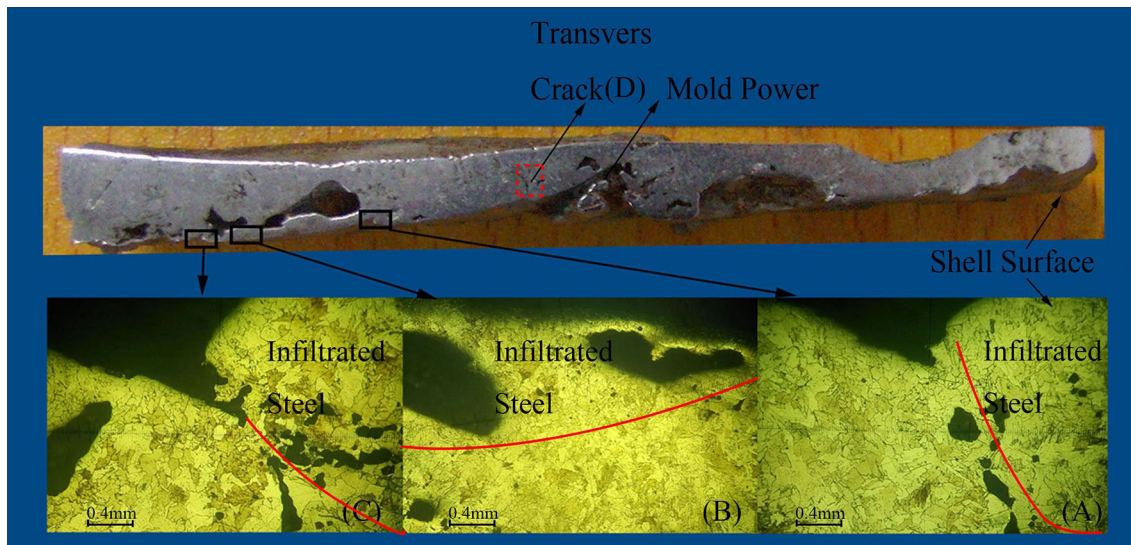Fig. 7—Contour map of the evolution of heat fluxes through mold hot surface.

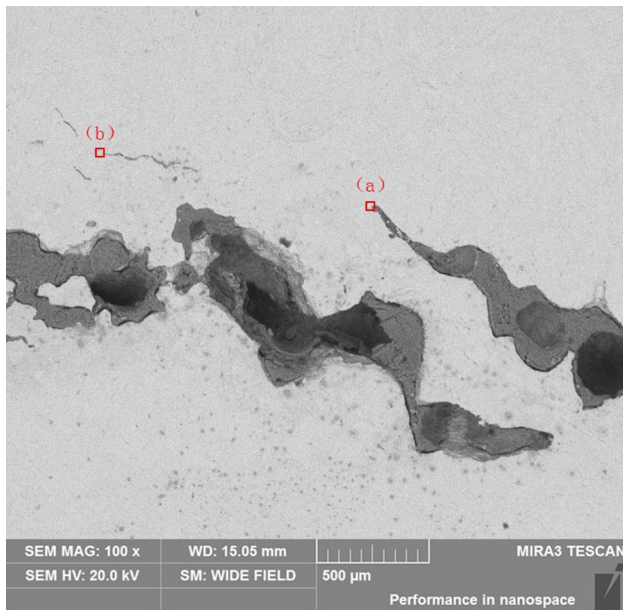Fig. 8—The cross section view of the initial solidified shell.

Fig. 9—Macro-morphology of transverse cracks across the side shell.

melts flow out of the shell and directly contact with the mold hot surface; thus the heat flux increases extremely. After the peak, the heat flux of S2 decreases as the melts flow downward leaving the air gap between shell and mold hot surface that introduces a sudden increase of thermal resistance.

The heat fluxes from S3 to S8 first decrease from 40 to 41 seconds due to the formation of interfacial thermal resistance with the solidification of molten steel, and then they increase rapidly from 42.2 seconds when the first breakout occurs at S2, as the fresh molten steel would overflow on the initial solidified surface of the shell that would strengthen the heat fluxes and the responding temperatures. It also can be proved by the overflowed solidified part at the bottom of the shell surface in Figure 4.

It is clearly shown that the heat flux of S2, S3, S4, and S5 reaches the peak in sequence at T1 = 42.2, T2 = 42.8, T3 = 43.4, and T4 = 44.5, respectively. Through tracing the moment of the heat flux peak and the given thermocouple space, the propagation velocity of the breakout can be computed by using the equation below.
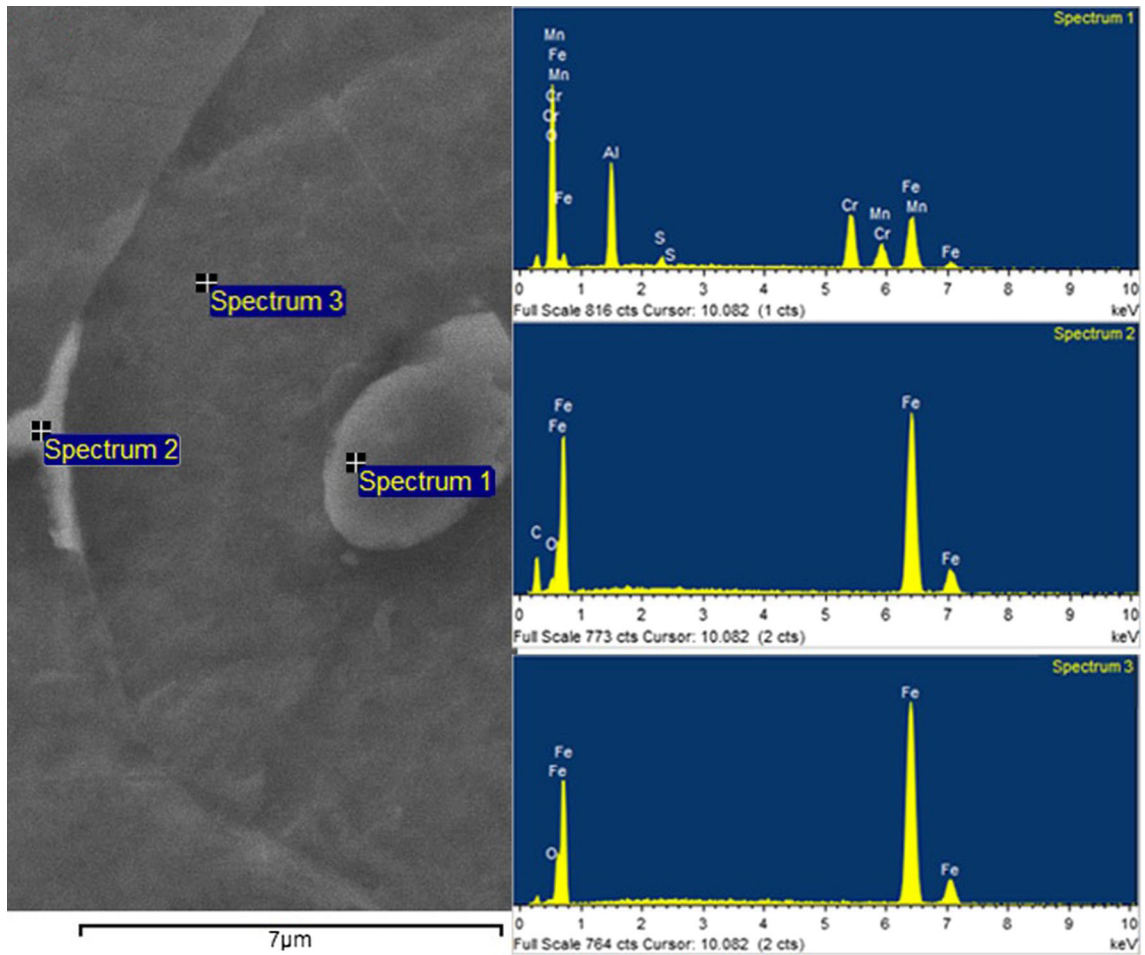

Fig. 10—Precipitations at position A analyzed by EDS.

$$v_y = \frac{D_y}{\Delta t_y},$$

where v_y is the vertical propagation velocity of the rupture point (m/min), D_y is the distance between the thermocouples in the copper mold (m), Δt_y is the time interval of the heat flux peak for the rupture point propagation in the vertical a direction (min). The average vertical propagation velocity of the rupture point is the calculated as 0.42 m/min (casting speed 0.6 m/min).

Figure 7 shows the mold displacement (D_m), velocity (V_m), and the contour map of the heat flux evolution across the mold hot surface during the cast period based on the calculation through 2D-IHCP. It turns out that the values for heat fluxes reach the maximum value also at about T1 = 42.2 seconds, T2 = 42.8 seconds, T3 = 43.4 seconds, and T4 = 44.2 seconds during positive strip tome (PST) of each oscillation cycle. Line a-b along the red area shows the trace of the rupture point movement. The vertical propagation velocity of the rupture can also be obtained though the following equation: $V_Y = \tan \alpha = 0.4$ m/min, and the value is similar to the calculated one above.

During one oscillation cycle, the mold oscillates sinusoidally along the equilibrium position; thus, the spheroidal protrusion will apply force on the shell periodically. The time when the mold moves downward faster than the casting speed is called negative strip time (NST), and the rest of the period is termed as positive strip time (PST). During the NST, the mold moves downward relative to the shell, the friction force exerted by the protrusion will be relatively small, as the movement of the shell and mold is in the same direction. However, the applied friction force will be large, when the mold is oscillated upward during the PST due to the fact that the movement of the mold and shell is opposite. Therefore, breakout is possibly occurred in PST, and the heat flux will peak correspondingly as shown in Figure 7.

B. *Surface Quality of the Shell*

In order to further analyze the quality of initial solidified shell that has been subjected to the external forces exerted by the protrusion, the shell is cut along the line AB in Figure 4, and the cross section of its side is shown in Figure 8. It is observed that severe oscillation marks and cracks are appearing along the shell side, where the mold powders and bubbles are entrapped under the hook-type oscillation marks. The overflowed steel solidified against the original shell and is shown in the locations of A, B, and C, where the holes and pores are observed to form inside it.

An obvious transvers crack is clearly shown at the location D across the side of shell in Figure 8, and its macro-morphology is shown in Figure 9. The EDS analysis for the position a, at the end of the transvers crack, and b along a micro-crack in Figure 9 is shown in Figures 10 and 11, individually. It can be observed that there is no carbonitrides precipitated around the corner of the macro-crack, as shown in Figures 10 and 11, as there is no second cooling and bending operations in
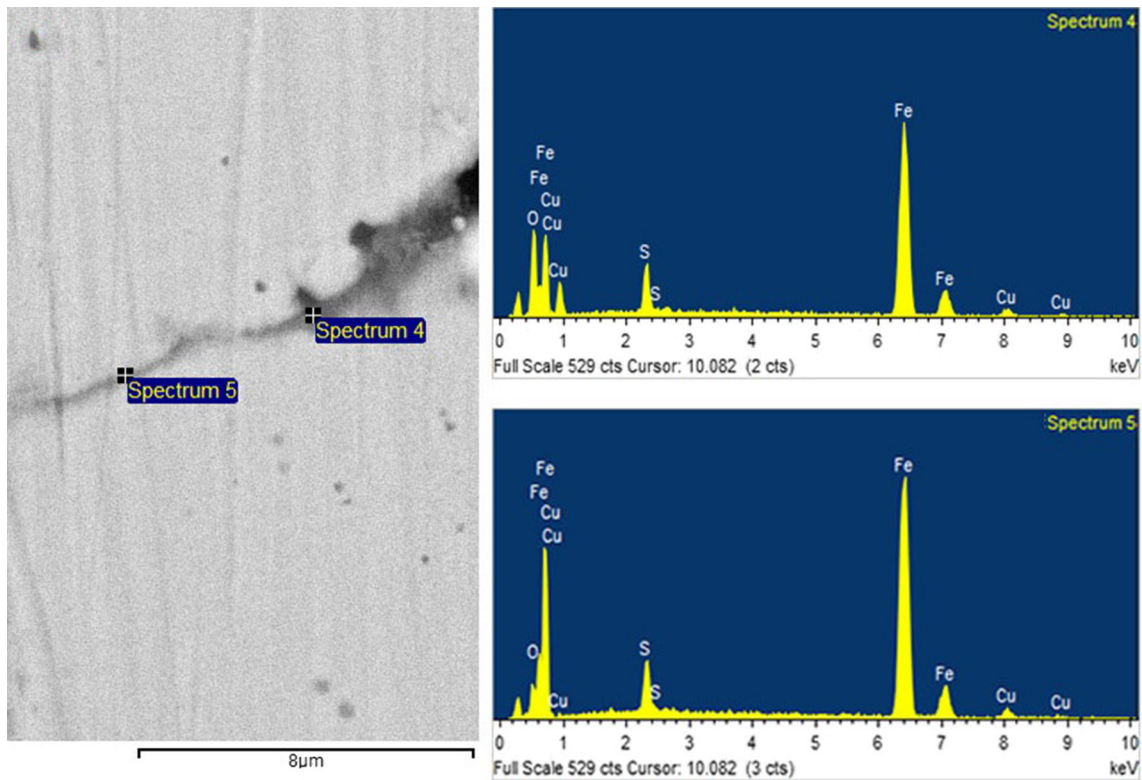

Fig. 11—Precipitation along micro-crack analyzed by EDS.

this simulation. However, sulfur is found to segregate along the cracks. It has been reported that the solute element S segregation or the precipitation of sulfide at the boundaries tends to reduce the grain-boundary strength and have a harmful influence on the strength, ductility, and solidification cracking sensitivity of steel.[22,23]

C. Mechanism of Breakout Based on this Simulator

Breakouts in continuous casting are associated with various factors, such as abnormal temperature gradient, inconsistent cast speed, insufficient lubrication between the mold and strand, and steel level fluctuation. In this paper, the external force exerted by the protrusion was applied to the initial shell to simulate the breakouts caused by friction between the mold and shell gap. In order to illustrate the mechanism of breakout formation based on this simulator, the schematic illustration of the shell and mold movement is shown in Figure 12.

First, the initial shell was formed on the water-cooling copper mold during the hold time from 40 to 41 seconds, and then the cast was initiated. Then the newly formed shell would be drawn downward, and was subjected to the external forces applied by the protrusion. When the cast started for 1 second at T1, 42.2 seconds (as shown in Figure 7), the hot mold surface would contact with the spheroidal protrusion during PST in an oscillation cycle; then the initial shell would be pushed towards the melt slightly as shown in Figure 12(b), where the initial shell was subjected to external horizontal force, ferrostatic pressure, and thermal stresses.
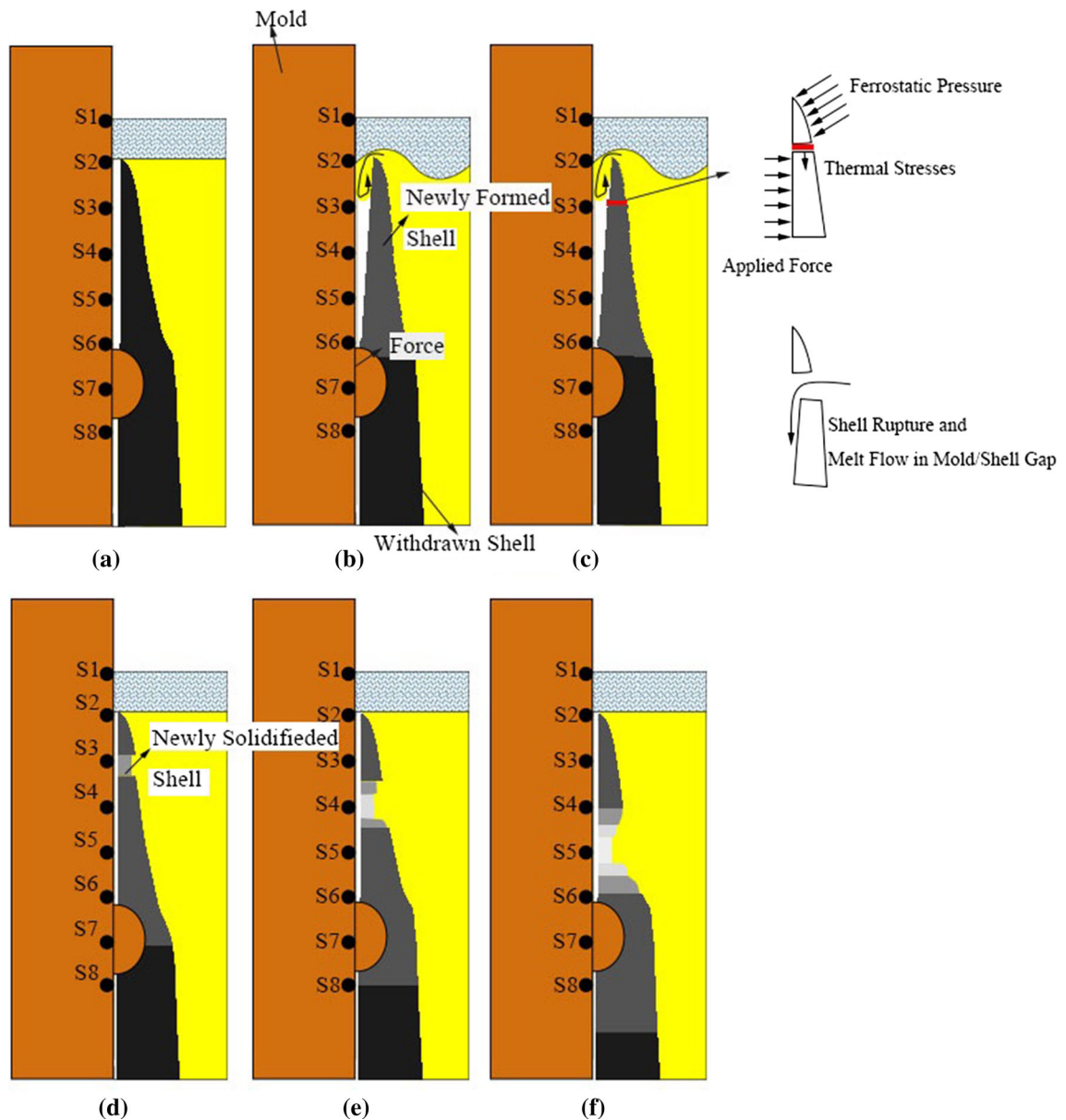

Fig. 12—Schematic diagram of the breakout formation and movement during cast. (a) Time = 41 s, (b) time = beginning of T1, (c) time = end of T1, (d) time = T2, (e) time = T3, (f) time = T4 (T1, T2, T3, and T4 were shown in Fig. 7).

Huge steel level fluctuation may be caused by this behavior and the liquid steel may overflow to the shell tip. Then the shell tip may be re-melted and it does not possess sufficient strength; therefore, breakout occurs at T1 due to the effects of above three forces as shown in Figure 12.

The fresh molten steel soon filled through the break point and solidified rapidly. The newly solidified shell is weak and it will be ruptured again during PST in the next oscillation cycles at T2, T3, and T4 as seen in Figure 7; the heat flux would then peak at each of these times during PST.

IV. CONCLUSION

A mold-cracking simulator has been successfully developed in this study to investigate the process of breakout and shell surface crack formation during the initial solidification of molten steel, and the specific conclusions are made as follows:

1. The responding temperatures in the mold were measured by two columns of thermocouples, and the results suggested that the breakout tends to introduce the peak of the responding temperature as the infiltrated fresh molten steel would directly contact the hot surface and heat the mold.
2. The evolution of heat fluxes across the mold surface has been calculated through a 2D-IHCD program, and it showed that the heat flux also tends to peak up at the same time when the breakout occurs. The relation between the mold displacement (Dm), velocity (Vm), and the contour map of the heat flux evolution across the mold hot surface clearly suggested that the breakouts usually occurred during PST period. The average vertical propagation velocity of the rupture point was calculated about 0.40 m/min.
3. Mold powders and bubbles were found to be entrapped in the deep hooks, and there was no carbonitrides precipitated around the corner of surface cracks; however, it was observed that sulfur is precipitated along the micro transvers cracks. It suggested that the segregation of sulfur during the initial solidification of molten steel does enhance the formation of micro transverse cracks.
4. A mechanism of breakout formation has been proposed based on the simulator results, and it indicates that the newly formed shell would be pushed towards the melt slightly, when the initial shell was cast downward, as it contacted with the spheroidal protrusion during PST in an oscillation cycle. Then the initial shell would be subjected to the external hori-

zontal force, ferrostatic pressure, and thermal stresses, and a huge steel level fluctuation may be caused that would introduce the overflow of liquid to the shell tip. Then the shell tip may be ruptured by above overall efforts, as it does not possess sufficient strength.

REFERENCES

1. K.C. Mills, T.J.H. Billany, A.S. Normanton, B. Walker, and P. Grieveson: *Ironmak. Steelmak.*, 1991, vol. 18, pp. 253–65.
2. M. Emi: *In Steelmaking Conference Proceedings*, 1991, Vol. 74, pp. 623–30.
3. Y. Mimura: Thesis, University of British Columbia, 1989.
4. A. Matsushita, M. Kato, W. Ohashi, M. Temma, and T. Syoji: *Trans. Iron Steel Inst. Jpn.*, 1985, vol. 25, p. 9.
5. D. Lee, C.H. Moon, S.C. Moon, and H.D. Park: *Control Eng. Pract.*, 2009, vol. 17, pp. 3–13.
6. S.K. Choudhary and S. Ganguly: *ISIJ Int.*, 2007, vol. 47, pp. 1759–66.
7. J. Sengupta, B.G. Thomas, H.J. Shin, G.G. Lee, and S.H. Kim: *Metall. Mater. Trans. A*, 2006, vol. 37A, pp. 1597–1611.
8. B.G. Thomas, J.K. Brimacombe, and I.V. Samarasekera: *Trans. Iron Steel Soc.*, 1986, vol. 7, pp. 7–20.
9. B. Mintz and D.N. Crowther: *Int. Mater. Rev.*, 2010, vol. 55, pp. 168–96.
10. J.K. Brimacombe and K. Sorimachi: *Metall. Mater. Trans. B*, 1977, vol. 8B, pp. 489–505.
11. G.I. Cardoso: Thesis, McGill University, 1990.
12. B. Weisgerber, K. Harste, and W. Bleck: *Steel Res. Int.*, 2004, vol. 75, pp. 686–92.
13. Y. Maehara, K. Yasumoto, Y. Sugitani, and K. Gunji: *Trans. Iron Steel Inst. Jpn.*, 1985, vol. 25, pp. 1045–52.
14. Y. Ohmori and T. Kunitake: *Met. Sci.*, 1983, vol. 17, pp. 325–32.
15. T. Kato, Y. Ito, M. Kawamoto, A. Yamanaka, and T. Watanabe: *ISIJ Int.*, 2003, vol. 43, pp. 1742–50.
16. B. Santillana: Thesis, Delft University of Technology, 2013.
17. H. Zhang, W. Wang, D. Zhou, F. Ma, B. Lu, and L. Zhou: *Metall. Mater. Trans. B*, 2014, vol. 45B, pp. 1038–47.
18. D. Zhou, W. Wang, H. Zhang, F. Ma, K. Chen, and L. Zhou: *Metall. Mater. Trans. B*, 2014, vol. 45B, pp. 1048–56.
19. H. Zhang, W. Wang, F. Ma, and L. Zhou: *Metall. Mater. Trans. B*, 2015, vol. 46B, pp. 2361–73.
20. H. Zhang and W. Wang: *Metall. Mater. Trans. B*, 2016, vol. 47B, pp. 920–31.
21. H. Zhang, W. Wang, and L. Zhou: *Metall. Mater. Trans. B*, 2015, vol. 46B, pp. 2137–52.
22. B. Mintz: *ISIJ Int.*, 1999, vol. 39, pp. 833–55.
23. G.A. Osinkolu, M. Tacikowski, and A. Kobylanski: *Mater. Sci. Technol. Lond.*, 1985, vol. 1, pp. 520–25.